Research Square

Preprints are preliminary reports that have not undergone peer review.
They should not be considered conclusive, used to inform clinical practice,
or referenced by the media as validated information.

An Integrative Computational and Experimental Approach to Characterizing Anti-Quorum Sensing and Anti-Biofilm Activities of Natural Compounds Targeting LuxS in Klebsiella pneumoniae

Mashego Jackson Mamosebo
University of the Witwatersrand
Suheena Ayrga
University of the Witwatersrand
Shabir Ahmed Madhi
University of the Witwatersrand
Shama Khan
Shama.Khan@nwu.ac.za

North-West University

Research Article

Keywords: Klebsiella pneumoniae, autoinducer-2 (AI-2), quorum sensing, biofilms, antimicrobial resistance

Posted Date: July 8th, 2026

DOI: https://doi.org/10.21203/rs.3.rs-10264818/v1

License: This work is licensed under a Creative Commons Attribution 4.0 International License. Read Full License

Additional Declarations: No competing interests reported.

Version of Record: A version of this preprint was published at Archives of Microbiology on September 15th, 2026. See the published version at https://doi.org/10.1007/s00203-026-05191-z.

Abstract

Introduction: Klebsiella pneumoniae

(KPn) has emerged as a major global health concern due to increasing antimicrobial resistance (AMR). The development of new antimicrobial agents is essential to address multidrug-resistant and emerging hypervirulent strains associated with increased morbidity and mortality worldwide.

Methods

In this study, an integrative computational–experimental approach was employed to characterise the anti-quorum sensing and anti-biofilm activities of selected natural compounds targeting the LuxS/autoinducer-2 (AI-2) system in KPn. Six compounds were initially screened using homology modelling, molecular docking, pharmacophore analysis, and molecular dynamics (MD) simulations.

Results

Resveratrol, quercetin, and epigallocatechin gallate showed favourable binding to LuxS. Although quercetin (ΔG_bind = − 45.47 kcal/mol) and epigallocatechin gallate (− 43.04 kcal/mol) exhibited stronger predicted affinities than resveratrol (− 39.22 kcal/mol), resveratrol demonstrated superior complex stability (RMSD: 1.8 ± 0.2 Å) and persistent interactions with key residues (Tyr63, Trp68). Experimental validation demonstrated that resveratrol exhibited significant antimicrobial activity (MIC/MBC = 32 µg/mL), significantly inhibited quorum sensing-associated phenotypes, and reduced KPn-*Acinetobacter baumannii* dual-species biofilm formation by 54.7%.

Conclusion

These findings identify resveratrol as a promising anti-virulence candidate and highlight the utility of integrative computational and experimental strategies for the identification of compounds targeting quorum sensing and biofilm formation in multidrug-resistant pathogens.

1. Introduction

Antimicrobial resistance (AMR) in bacterial infections is estimated to be associated with approximately 5.0 million deaths annually, of which 4.3 million occur in low- and middle-income countries (LMICs) (Murray et al. 2022). The escalating crisis of morbidity and mortality due to AMR bacteria has rendered many conventional antibiotics increasingly ineffective, necessitating the development of alternative therapeutic strategies that extend beyond traditional bactericidal approaches (Bengtsson-Palme et al. 2018).

The ESKAPE pathogens (*Enterococcus faecium, Staphylococcus aureus, Klebsiella pneumoniae, Acinetobacter baumannii, Pseudomonas aeruginosa*, and *Enterobacter species*) are among the most clinically significant AMR bacterial pathogens. In particular, *Klebsiella pneumoniae* (KPn) has been designated a critical priority pathogen by the World Health Organization (WHO) (World Health Organization 2024). *Klebsiella pneumoniae*, a Gram-negative bacterium, is a major cause of hospital-acquired infections, including pneumonia, bloodstream infections, urinary tract infections, and meningitis, with case fatality risk exceeding 40% when associated with multidrug-resistant (MDR) strains (Chen et al. 2024). The prominence of KPn is attributed not only to extensive antimicrobial resistance mechanisms, including extended-spectrum β-lactamases and carbapenemases (Liang et al. 2022), but also to its ability to form biofilms that enhance persistence, immune evasion, and horizontal gene transfer (Olwagen et al. 2025).

Biofilm formation and virulence in KPn are closely associated with quorum sensing (QS), a cell-density-dependent communication system that regulates gene expression (Deryabin et al. 2019). Unlike many Gram-negative bacteria that rely on acyl-homoserine lactone (AHL)-based systems, KPn predominantly utilises the LuxS/autoinducer-2 (AI-2) pathway for intercellular communication (Chen et al. 2020). The LuxS enzyme catalyses the production of AI-2, linking quorum sensing with central metabolism through the activated methyl cycle (Schauder et al. 2001). The AI-2 system plays a key role in regulating biofilm formation, virulence factor expression, and plasmid-mediated gene transfer thereby making LuxS an attractive target for anti-virulence therapy (Hall-Stoodley et al. 2004).

Multiple strategies have been developed to disrupt the LuxS/AI-2 system at distinct mechanistic levels, including substrate analogues such as S-adenosyl-L-homocysteine (SAH), which competitively inhibits LuxS by mimicking its natural substrate S-ribosylhomocysteine (SRH), thereby reducing AI-2 synthesis. Additional approaches involve synthetic DPD analogues that interfere with AI-2 receptor binding, ribose-based intermediates that disrupt catalytic function through structural mimicry, and metal-chelating agents that impair the zinc-dependent enzymatic activity of LuxS (Roy et al. 2011). Collectively, these strategies reinforce the feasibility of targeting LuxS as a means of modulating quorum sensing and attenuating virulence without directly affecting bacterial viability.

Targeting QS represents a promising strategy to disarm pathogens without exerting strong selective pressure for resistance. Natural compounds, including flavonoids and polyphenols such as quercetin, resveratrol, epigallocatechin gallate (EGCG), and curcumin, have demonstrated the ability to interfere with QS signaling, disrupt biofilms, and attenuate virulence through diverse mechanisms (Rutherford and Bassler 2012). Nevertheless,

experimental screening of large compound libraries is resource-intensive, highlighting the importance of computational approaches for prioritising promising candidates.

Target-based molecular docking enables rapid identification of compounds with high binding affinity to specific targets, while molecular dynamics (MD) simulations provide insight into the stability and dynamic behaviour of protein–ligand complexes under physiological condition. When combined with pharmacokinetic (ADMET) profiling, these approaches facilitate efficient prioritisation of compounds with favourable drug-like properties (Khan et al. 2024).

In this study, an integrative computational-experimental framework was employed to identify and evaluate natural compounds targeting the LuxS enzyme in KPn. Computational modelling, including homology modelling, molecular docking, pharmacophore analysis, and MD simulations, was used to prioritise candidate compounds. These compounds were subsequently evaluated in vitro for their antimicrobial, quorum-sensing inhibitory, and anti-biofilm activities. Quorum-sensing inhibition was assessed using a *Chromobacterium violaceum* (*C. violaceum*) biosensor system, which provides a convenient phenotypic indicator of QS interference through violacein production. While this system primarily reflects AHL-mediated signalling, it serves as a general screening tool for QS disruption rather than a direct measure of LuxS/AI-2 pathway inhibition in KPn. S-adenosyl-L-homocysteine (SAH) was employed as a quorum-sensing inhibitory control to provide a reference for LuxS-targeted activity. Its inclusion enables direct comparison of candidate compounds against a well-characterised anti-virulence reference, allowing specific evaluation of quorum-sensing-targeted effects independent of bactericidal activity. By integrating computational predictions with phenotypic validation, this study presents a systematic approach for identifying potential anti-virulence agents targeting quorum sensing and biofilm formation in multidrug-resistant KPn.

2. Methods and Materials

This study employed an integrative computational-experimental approach to characterise natural compounds with anti-quorum-sensing (QS) and anti-biofilm activity against KPn. The workflow comprised (i) in silico modelling and screening targeting the LuxS enzyme, followed by (ii) in vitro validation of selected compounds using antimicrobial, anti-QS, and biofilm inhibition assays. This combined strategy enabled both mechanistic prediction and functional validation of anti-virulence-associated activity.

In silico Predictions

Software and Computational Resources

Molecular docking and molecular modelling were performed using the Schrödinger Maestro suite (Release 2023-2, Schrödinger LLC, USA). Molecular dynamics (MD) simulations were conducted using the AMBER 18 package with GPU acceleration. All computations were performed on the Centre for High Performance Computing (CHPC), Cape Town, South Africa.

Target Sequence Retrieval and Template Selection

The amino acid sequence of S-ribosylhomocysteine lyase (LuxS) from KPn (UniProt accession: B5XVC4) was retrieved from UniProtKB. Template identification was performed using BLASTP against the Protein Data Bank (PDB). The crystal structure of LuxS from *Salmonella enterica* serovar Typhi (PDB ID: 5E68; resolution 1.80 Å) (Guan et al. 2015)was selected as a template based on high sequence identity (91%), coverage (98%), and a significant E-value (2×10^{-80}).

Homology Modelling and Validation

Homology modelling was conducted using the Prime module in Schrödinger. Sequence alignment was performed using ClustalW, and model construction employed an energy-based approach incorporating loop refinement and side-chain optimisation. The zinc cofactor present in the template was retained. Model validation was performed using the SAVES server (https://saves.mbi.ucla.edu/), including PROCHECK (Ramachandran analysis), ERRAT, VERIFY_3D and WHATCHECK. Structural agreement was further assessed by comparison with the AlphaFold-predicted LuxS structure.

Protein and Ligand Preparation

The LuxS model was prepared using the Protein Preparation Wizard in Schrödinger. Hydrogen atoms were added, bond orders assigned, and protonation states optimized at physiological pH using Epik (Shelley et al. 2007). Energy minimisation was conducted using the OPLS-2005 (41) force field with a convergence threshold of 0.30 Å RMSD. Six natural compounds (quercetin, curcumin, epigallocatechin gallate (EGCG), allicin, resveratrol, and berberine) were selected based on reported QS inhibitory activity, structural diversity, and availability. S-adenosyl-L-homocysteine (SAH) was included as a reference LuxS inhibitor. Ligands were prepared using LigPrep, including ionisation state prediction (pH 7.0 ± 2.0), tautomer generation, stereoisomer enumeration, desalting, and energy minimisation using the OPLS-2005 force field.

Identification of Pharmacophore Hypothesis

A structure-based e-pharmacophore modelling approach was employed using the PHASE module (42). Six standard pharmacophoric features were considered: hydrogen bond acceptors (A), hydrogen bond donors (D), hydrophobic groups (H), negatively ionisable groups (N), positively ionisable

groups (P), and aromatic rings (R). An energy-optimised pharmacophore (e-pharmacophore) was derived based on the docked conformation of S-adenosyl-L-homocysteine (SAH) within the LuxS active site. The model incorporated key interaction features, including hydrogen bonding and hydrophobic interactions. Excluded volumes were defined around the bound ligand to represent steric constraints of the active site. Pharmacophore features were selected based on critical interactions with key active-site residues involved in ligand binding. The resulting pharmacophore model captured the essential structural features required for effective interaction with the LuxS active site (Dixon et al. 2006).

Molecular Docking

The Glide-based docking module of the Schrödinger suite was employed to identify compounds with strong binding affinity toward the LuxS protein. A receptor grid was generated around the active site using an outer grid box of 30 × 30 × 30 Å and an inner grid box of 18 × 18 × 18 Å to ensure accurate ligand sampling within the binding pocket. The compound library was subjected to a hierarchical two-stage docking protocol, comprising Standard Precision (SP) followed by Extra Precision (XP) docking. Top candidates were selected based on XP GlideScore ranking and favourable interaction profiles. A cutoff of -6 kcal/mol was applied, and compounds with GlideScores ≤ -6 kcal/mol were retained for further analysis. Complexes exhibiting more negative binding scores and consistent interactions with key active-site residues were prioritised, indicating higher predicted binding stability. Berberine did not localise within the catalytic pocket and consistently occupied alternative regions, suggesting a different binding preference, and was therefore excluded from downstream analysis.

ADMET and Drug-Likeness Prediction

Pharmacokinetic profiles were predicted using QikProp 5.6 including molecular weight, hydrogen bond donors and acceptors, octanol/water partition coefficient (logP), polar surface area (PSA), aqueous solubility (logS), Caco-2 cell permeability, blood–brain barrier penetration (logBB), human oral absorption and potential cardiotoxicity (hERG channel inhibition). Drug-likeness was assessed using Lipinski's Rule of Five (Lipinski et al. 2001).

Molecular Dynamics (MD) Simulations

All atom MD simulations(Salsbury 2010) were performed for selected compounds (resveratrol, quercetin, EGCG) and SAH using AMBER18 tools (Case et al. 2023). Systems were parameterised using the ff14SB force field for the protein(Maier et al. 2015) and General AMBER Force Field (GAFF) for ligands, solvated in a TIP3P water box, and neutralised with counterions. Long-range electrostatic interactions were treated using the Particle Mesh Ewald (PME) method with a non-bonded cut-off of 12 Å. The SHAKE algorithm constrained all bonds involving hydrogen atoms, enabling a 2-fs integration time step. Energy minimisation was performed in two stages: 2500 steps of steepest descent followed by 1500 steps of conjugate gradient minimisation, initially with positional restraints that were gradually reduced. Systems were heated from 0 K to 300 K under constant volume with weak harmonic restraints (10 kcal$\cdot\ \mathrm{mol}^{-1}\cdot\ \backslash\mathrm{AA}\backslash:^{-2}$), followed by density equilibration (50 ps, Berendsen barostat) and constant-pressure equilibration (500 ps, 1 atm, 300 K). A 100 ns production run was performed under NPT conditions. Trajectories were analysed using CPPTRAJ for RMSD, RMSF, radius of gyration, and solvent-accessible surface area (Roe and Cheatham 2013).

Binding Free Energy Calculations (MM/GBSA)

Binding free energy was estimated using the MM/GBSA method from the final 50 ns of MD trajectories (Genheden and Ryde 2015). The binding free energy ($\Delta\ G_{\mathrm{bind}}$) was calculated as:

$$\Delta\ G_{\mathrm{bind}} = G_{\mathrm{complex}} - G_{\mathrm{protein}} - G_{\mathrm{ligand}}$$

where $G = E_{\mathrm{gas}} + G_{\mathrm{solvation}} - TS$. The entropic term ($-TS$) was excluded as it is computationally expensive and contributes minimally to relative binding energy comparisons. The gas-phase energy (E_{gas}) comprises internal, van der Waals, and electrostatic contributions:

$$E_{\mathrm{gas}} = E_{\mathrm{int}} + E_{\mathrm{vdW}} + E_{\mathrm{elec}}$$

Solvation free energy ($G_{\mathrm{solvation}}$) includes polar and non-polar components:

$$G_{\mathrm{solvation}} = G_{\mathrm{polar}} + G_{\mathrm{nonpolar}}$$

Polar solvation energy was calculated using the Generalized Born (GB) model (dielectric constants: 1.0 for solute, 80.0 for solvent). Non-polar solvation energy was estimated from SASA:

$$G_{\mathrm{nonpolar}} = \gamma\ \cdot\ \mathrm{SASA} + \beta$$

$$\text{where } \gamma = 0.00542\ \mathrm{kcal}\cdot\mathrm{mol}^{-1}\cdot\mathrm{Å}^{-2} \text{ and } \beta = 0\ \mathrm{kcal}\cdot\mathrm{mol}^{-1} (54)$$

In Vitro Experiments

Bacterial Strains, Culture Conditions and Compound Preparations:

Compounds selected from computational screening were prioritised for experimental validation based on binding affinity, stability, and predicted pharmacokinetic properties. A reference strain (KPn ATCC 13883), a clinical multidrug-resistant (MDR) KPn isolate, and an MDR *Acinetobacter baumannii* isolate were used (a WHO critical priority pathogen frequently co-isolated with KPn) to assess interspecies biofilm disruption (Thakur et al. 2025). A biosensor strain, *Chromobacterium violaceum*, was used for anti-quorum sensing (AQS) assays. Cultures were maintained as glycerol stocks at − 80°C and revived on LB or BHI agar. Working cultures were prepared in Mueller-Hinton broth (MHB) or Luria-Bertani (LB) broth and standardised to OD_{600} = 0.1 (~ 10^8 CFU/mL). Quercetin, resveratrol, and EGCG were selected based on computational screening. Stock solutions were prepared in DMSO (or PBS for SAH), filter-sterilised, and used at final solvent concentrations ≤ 2% (v/v).

Antibacterial Activity (MIC and MBC)

Minimum inhibitory concentrations (MICs) were determined using the broth microdilution method in 96-well plates according to CLSI guidelines. Serial dilutions (1024–0.5 µg/mL) were prepared, and bacterial inocula (~ 5 × 10^5 CFU/mL) were added. After incubation (16–20 h, 35°C), viability was assessed using p-iodonitrotetrazolium violet (INT). MIC was defined as the lowest concentration preventing colour change. Minimum bactericidal concentrations (MBCs) were determined by plating aliquots from MIC wells onto agar. A ≥ 3 $\log_{10}$ reduction in CFU was considered bactericidal.

Anti-Quorum Sensing Assays

A biosensor strain, *C. violaceum*, was utilized due to its well-characterised violacein production system. This strain serves as a convenient biosensor for detecting quorum-sensing inhibition through violacein production. While this system primarily reflects AHL-mediated signalling, it serves as a general screening tool for QS interference rather than a direct measure of LuxS/AI-2 pathway inhibition in KPn.

Qualitative and Quantitative Violacein Assay

Agar well diffusion assays were performed using *C. violaceum*. Wells were loaded with compounds at MIC concentrations, and plates were incubated at 30°C for 24 h. Zones of pigment inhibition (without growth inhibition) were measured. Violacein inhibition was quantified in microtiter plates. After incubation, pigment was extracted with DMSO, and absorbance was measured at 485 nm. Percentage inhibition was calculated relative to untreated controls, and IC_{50} values were determined using nonlinear regression.

Biofilm Inhibition Assay

Biofilm formation was assessed in 96-well plates using single- and dual-species models. Compounds were tested at sub-MIC concentrations. After 24 h incubation, biofilms were stained with crystal violet, and absorbance was measured at 590 nm. Biofilm inhibition (%) was calculated relative to untreated controls, and the minimum biofilm inhibitory concentration (MBIC) was defined as ≥ 50% inhibition.

Viable Cell Counting on Selective Media

Biofilms were resuspended, serially diluted, and plated on selective media to determine CFU/mL for each species. Log reductions were calculated relative to controls.

Statistical Analysis

All experiments were conducted in triplicate across three independent replicates (n = 3). Data are presented as mean ± standard deviation. Statistical analyses were performed using GraphPad Prism 9.0. One-way ANOVA with Dunnett's test and two-way ANOVA with Tukey's test were used as appropriate. Pearson correlation analysis was performed to enable integration of computational predictions with experimental outcomes. Statistical significance was set at $p < 0.05$.

3. Results and Discussion

In silico Results

3.1 Homology Modelling and Validation

To our knowledge, the three-dimensional structure of the LuxS protein from KPn has not been reported in publicly available databases. Therefore, a homology modelling approach was employed to generate the LuxS structure. The LuxS protein from *Salmonella enterica* (PDB ID: 5E68) was selected as the template due to its high sequence identity (91%) and structural conservation. The generated model exhibited the characteristic TIM-barrel $(\beta/\alpha)_8$ fold with the catalytic zinc ion correctly positioned within the active site. Validation of the model showed favourable structural quality, with an ERRAT score of 94.27% and 86.42% of residues passing VERIFY3D thresholds. The ProSA Z-score (− 5.62) was within the range of experimentally determined structures, while Ramachandran analysis confirmed that 91.4% of residues were in the most favoured regions with no residues in disallowed regions. These results indicate that the generated LuxS model is reliable and suitable for downstream computational analysis.

3.2Molecular Docking of Natural Compounds

Molecular docking was performed to evaluate the binding affinity of selected natural compounds towards the LuxS protein, using S-adenosyl-L-homocysteine (SAH) as a reference inhibitor (Table 1).

Table 1
Glide XP docking scores (kcal/mol) of selected natural compounds and the reference ligand SAH against the LuxS active site.

Compounds	XP Score (kcal/mol)
Resveratrol	-8.51
Quercetin	-8.01
Epigallocatechin gallate (EGCG)	-7.58
S-adenosyl-L-homocysteine (SAH)	-6.78
Curcumin	-5.21
Allicin	-5.03

Among the tested compounds, resveratrol showed the strongest binding affinity with a docking score of − 8.51 kcal/mol, followed by quercetin (-8.01 kcal/mol) and epigallocatechin gallate (EGCG) (-7.58 kcal/mol). All three compounds exhibited more favourable binding scores compared to SAH (-6.78 kcal/mol), indicating stronger interactions within the active site.

Two-dimensional interaction maps (Fig. 1) illustrate the binding interactions of the selected compounds with key active-site residues of LuxS. These interactions include hydrogen bonds, hydrophobic contacts, and electrostatic interactions involving residues such as Glu50, Glu57, His54, Ile53, Met81, Met133, Pro80, Gly82, and Arg84. Conserved interaction patterns were observed across compounds, with resveratrol showing favourable positioning within the catalytic pocket and consistent hydrogen bonding with key residues. Based on these findings, resveratrol, quercetin, and EGCG were selected for further analysis.

3.3 Structure-Based Pharmacophore Modelling

A structure-based e-pharmacophore model was generated using the docked conformation of SAH within the LuxS active site (Fig. 2). The model identified key interaction features, including hydrogen bond donors (blue arrows), hydrogen bond acceptors (red arrows), and aromatic ring interactions (orange spheres). Excluded volumes (grey spheres) represent steric constraints of the binding pocket. The selected compounds, particularly resveratrol and quercetin, showed good alignment with the pharmacophore features, suggesting that these molecules possess the required structural characteristics for effective interaction with the LuxS active site.

3.4 ADMET Analysis:

The drug-likeness and pharmacokinetic properties of the selected compounds were evaluated using QikProp. Resveratrol and quercetin complied with Lipinski's Rule of Five with no violations, indicating favourable oral bioavailability, whereas epigallocatechin gallate (EGCG) and S-adenosylhomocysteine (SAH) each showed violations, mainly due to higher polarity and molecular size. As shown in Table 2, the qualitative human oral absorption score (scale 1–3) aligned with polar surface area (PSA). Resveratrol (PSA 56.6 Å²) and quercetin (91.9 Å²) were both assigned the highest absorption category (3), while EGCG (PSA 138.1 Å²) was predicted as moderate (2) and SAH (PSA 123.0 Å²) as low (1). Consistent with these trends, Caco-2 permeability (QPPCaco) was exceptionally high for resveratrol (395.7 nm s^{-1}), confirming a strong ability to traverse intestinal epithelia, whereas EGCG (13.7 nm s^{-1}) and SAH (6.3 nm s^{-1}) showed limited permeability. Predicted aqueous solubility (QPlogS) was highest for resveratrol (− 1.15) and quercetin (− 2.50), while EGCG (− 5.80) and SAH (− 2.02) were less soluble. Octanol/water partitioning (QPlogPo/w) reflected the polarity differences, with EGCG being the most lipophilic (2.72) and SAH the most hydrophilic (− 2.49). Brain penetration estimates (CNS activity and QPlogBB) indicated that all compounds are unlikely to enter the CNS; resveratrol gave a modest CNS score of − 1 and a QPlogBB of − 0.81, whereas the others were strongly restricted. The hERG inhibition risk (QPlogHERG) was within acceptable limits. Resveratrol demonstrated high predicted permeability and favourable solubility, while EGCG exhibited lower permeability despite acceptable binding affinity. These findings suggest that resveratrol and quercetin may have better pharmacokinetic profiles compared to EGCG.

Table 2
In-silico ADME/T predictions of the selected compounds.

Compounds Names	CNS	QPlogKhsa	SASA	QPlogPo/w	QPlogS	QPlogBB	QPlogHERG	QPPCaco	PSA	Rule Of Five	Human Oral Absorption
EGCG	-2	0.616	634.058	2.720	-5.797	-3.345	-5.649	13.723	138.055	2	2
Quercetin	-2	-0.459	455.789	0.409	-2.498	-2.074	-4.796	58.843	91.896	0	3
Resveratrol	-1	-0.615	353.509	0.302	-1.147	-0.807	-3.004	395.735	56.629	0	3
SAH	-2	-1.167	617.131	-2.490	-2.015	-2.461	-6.481	6.310	122.974	2	1

3.5 Molecular Dynamics Simulation Analysis: Structural Stability, Flexibility, Compactness, and Solvent Exposure

To evaluate the dynamic stability and conformational behaviour of the LuxS protein in complex with selected ligands, 100 ns molecular dynamics (MD) simulations were performed.

Structural stability was assessed using the RMSD of Cα backbone atoms over the 100 ns trajectory (Fig. 3A). All complexes reached equilibrium within the initial phase of the simulation and remained stable throughout the trajectory. The LuxS-resveratrol complex exhibited the lowest deviation (1.8 ± 0.2 Å), indicating higher structural stability compared to other complexes. The LuxS-quercetin and LuxS-EGCG complexes showed slightly higher deviations (2.1 ± 0.3 Å and 2.4 ± 0.4 Å), suggesting comparatively flexible interactions. The SAH complex remained stable but displayed less compact behaviour over time. Residue-level flexibility analysis (Fig. 3B) revealed reduced fluctuations in key active-site regions (residues 50–70 and 120–140) for the LuxS-resveratrol complex, indicating stable binding interactions. In contrast, LuxS-EGCG exhibited the highest fluctuations in loop regions, suggesting less stable interaction over time. While the LuxS-SAH complex remained steady, LuxS-quercetin demonstrated intermediate flexibility, particularly in the peripheral loops.

The radius of gyration (Rg) analysis showed the LuxS–resveratrol complex maintained the most compact structure (Rg 18.3 ± 0.1 Å) and lowest solvent exposure throughout the simulation. Similarly, SASA analysis showed reduced solvent exposure (above 15,500 Å²) for this complex compared to the reference, supporting improved structural stability (19.4 ± 0.3 Å). These findings suggest that resveratrol promotes a more stable and compact protein conformation. The Rg and SASA values were corrected to align with the scale in Fig. 3C and D.

3.6 Hydrogen Bond and Principal Component Analysis (PCA)

Hydrogen bonding patterns were analysed over the final 100 ns of the trajectories (Fig. 5). The LuxS–resveratrol complex formed stable hydrogen bonds with key active-site residues (e.g., Tyr63 and Trp68), along with π–π interactions that contributed to its stability. LuxS–quercetin showed fewer persistent interactions, while LuxS–EGCG exhibited more variable bonding patterns. The LuxS–SAH complex formed the fewest stable hydrogen bonds, correlating with reduced stability. Principal component analysis (PCA) was performed to characterise large-scale conformational motions. Projection onto PC1 and PC2 (Fig. 4) revealed that the LuxS–resveratrol complex occupied a more confined conformational space, indicating restricted motion and enhanced stability. This restricted motion is indicative of enhanced stability and reduced structural flexibility. LuxS–quercetin and LuxS–EGCG showed broader distributions, reflecting greater conformational flexibility.

3.7 Secondary Structure Analysis

Secondary structure analysis was performed to assess the impact of ligand binding on the structural integrity of the LuxS protein during the 100 ns simulation. Overall, all complexes retained their characteristic secondary structural elements, with dominant α-helical and β-sheet regions remaining largely preserved throughout the trajectory. Secondary structure composition (Table 3) indicated that the LuxS-resveratrol complex preserved the highest α-helical content and lowest loop fraction, reflecting stabilisation of the native fold. LuxS–quercetin and LuxS–EGCG showed moderate structural perturbations, whereas LuxS-SAH bound system showed moderate stability but displayed more variability compared to the resveratrol complex (Fig. 6).

These findings suggest that ligand binding does not disrupt the structure of LuxS and further support the enhanced structural stability observed for the resveratrol-bound complex, consistent with RMSD and RMSF analyses.

Table 3
Percentage of residues contributing to the secondary structure of LuxS protein in complex with studied inhibitors and control inhibitor calculated after 100 ns of MD trajectories.

Protein-ligand complex	α	B	3_{10}-Helix	Turn	Bend	Other
SAH-LuxS	25	19	12	12	13	19
Res-LuxS	23	24	8	15	14	16
Que-LuxS	26	26	11	9	13	15
EGCG-LuxS	25	23	10	11	12	19

3.8 Binding Free Energy Calculations (MM/GBSA)

Binding free energies calculations showed that quercetin had the most favorable binding affinity (ΔG_bind = − 45.47 kcal/mol), followed by EGCG (–43.04 kcal/mol) and resveratrol (–39.22 kcal/mol), all outperforming the reference SAH (–33.04 kcal/mol). The strong binding affinity of quercetin and EGCG was primarily driven by favourable gas-phase interactions, including van der Waals and electrostatic contributions. However, these interactions were partially offset by higher solvation penalties. In contrast, resveratrol displayed a more balanced energetic profile, with strong van der Waals interactions and comparatively lower solvation penalties. Notably, despite its slightly lower binding affinity, resveratrol demonstrated enhanced structural stability in MDS, highlighting the importance of considering both binding energetics and dynamic behaviour in ligand prioritisation. This observation suggests that dynamic stability may play a more important role than static binding affinity in determining biological activity.

Table 4
Binding free energy calculations of LuxS protein in complex with S-adenosyl-L-homocysteine (SAH), Resveratrol (Res), Quercetin (Que) and Epigallocatechin gallate (EGCG) inhibitors using MM/GBSA approach.

Protein-ligand complex	ΔEvdW	ΔEele	ΔGgas	ΔGpolar	ΔGnonpolar	ΔGsol	ΔGbind
SAH-LuxS	-24.63	-4.40	-28.04	21.12	-4.37	16.75	-33.04
Res-LuxS	-35.43	-5.87	-38.12	24.71	-7.61	17.10	-39.22
Que-LuxS	-29.36	-5.16	-39.44	23.71	-6.71	17.00	-45.47
EGCG-LuxS	-32.33	-8.30	-43.44	22.38	-6.37	16.01	-43.04

In Vitro Validation

Based on the computational analysis, resveratrol, quercetin, and EGCG were selected for experimental validation. SAH was included as a reference compound to assess assay performance.

3.9 Antibacterial Activity (Viable Cell Reduction and MIC/MBC)

The antibacterial activity of the selected compounds was assessed using MIC and MBC assays and the results are summarised in Table 4 and Fig. 7. Resveratrol exhibited the highest activity, achieving approximately a 5-log reduction in CFU/mL, indicating strong bactericidal effects. EGCG demonstrated moderate activity, with a reduction slightly above 3 logs, suggesting effective but comparatively lower antibacterial potency. In contrast, quercetin and SAH showed limited activity, with reductions below 2 logs. Consistent with these findings, MIC and MBC assays revealed that resveratrol exhibited the strongest antibacterial activity (MIC/MBC = 32 µg/mL), indicating bactericidal behaviour. EGCG also showed bactericidal activity, although at a higher concentration (256 µg/mL). In contrast, quercetin and SAH demonstrated bacteriostatic effects, with MIC values of 512 µg/mL and MBC values exceeding 1024 µg/mL (MBC:MIC > 2). Collectively, these results indicate that resveratrol is the most effective compound, demonstrating the highest antibacterial potency and reduction in bacterial viability among the tested compounds.

Table 5
Minimum Inhibitory Concentration (MIC) and Minimum Bactericidal Concentration (MBC) of Test Compounds Against KPn ATCC 13883 strain.

Compound	MIC (µg/mL)	Log_{10} Reduction at MIC	MBC (µg/mL)	MBC:MIC Ratio	Classification
Resveratrol	32	> 4.7	32	1	Bactericidal
EGCG	256	> 3.0	256	1	Bactericidal
Quercetin	512	1.7	> 1024	> 2	Bacteriostatic
SAH	512	1.7	> 1024	> 2	Bacteriostatic

3.10 Anti-Quorum Sensing Activity

The anti-quorum sensing activity of the compounds was assessed using the *Chromobacterium violaceum* biosensor system. All compounds showed measurable inhibition of violacein production, indicating interference with quorum sensing pathways. Resveratrol exhibited the highest activity (23.0 mm), showing near-complete inhibition at MIC and the lowest IC_{50} value of 110 µM. Quercetin (19.5 mm) and EGCG (17.0 mm) showed moderate inhibitions, with IC_{50} values of 199 µM (80% inhibition) and 251 µM (60% inhibition) respectively, while SAH demonstrated weaker activity (Table 6; Fig. 8). The SAH control validated the assay with a reliable but weak IC_{50} >1000 µM. These metrics align with the computational predictions, confirming the hierarchy of anti-QS efficacy.

Table 6
Anti-Quorum Sensing Activity of Test Compounds Against *Chromobacterium violaceum.*

Compound	Zone Diameter (mm)	CLSI Classification	IC_{50} (µM)	% Inhibition at MIC	QS Potency Classification
Resveratrol	23.0	Susceptible (S)	110 µM	99.8%	Moderate
EGCG	17.0	Intermediate (I)	251 µM	60%	Weak
Quercetin	19.5	Intermediate (I)	199 µM	80%	Moderate (borderline)
SAH	18.5	Intermediate (I)	> 1000 µM	70% (at 1 mM)	Very Weak (Reference)

3.11 Biofilm Inhibition:

Biofilm inhibition assays revealed that resveratrol significantly reduced biofilm formation at sub-MIC (8 µg/mL) concentrations, achieving over 50% inhibition. Quercetin (128 µg/mL) and EGCG (64 µg/mL) showed moderate effects with biomass inhibition of 35.2% and 29.7% respectively, while SAH exhibited minimal activity (1 mM; 20.3% inhibition) (Table 7; Fig. 9). Interestingly, *A. baumannii* was more susceptible to biofilm disruption compared to KPn, suggesting possible differences in quorum sensing regulation or compound uptake between species.

Table 7
Inhibition of Dual-Species Biofilm Formation by Test Compounds.

Compound	Concentration (1/4 MIC)	Biofilm Biomass (OD_{590})	% Inhibition	Log_{10} Reduction (*Kp* ATCC)	Log_{10} Reduction (*Kp* Clinical)	Log_{10} Reduction (*Ab*)
Untreated Control	-	1.28 ± 0.14	-	-	-	-
Resveratrol	8 µg/mL	0.58 ± 0.06	54.7%	1.1 ± 0.2	1.0 ± 0.2	1.6 ± 0.3
EGCG	64 µg/mL	0.90 ± 0.11	29.7%	0.4 ± 0.1	0.3 ± 0.1	0.6 ± 0.2
Quercetin	128 µg/mL	0.83 ± 0.10	35.2%	0.5 ± 0.2	0.4 ± 0.2	0.8 ± 0.2
SAH (Control)	1 mM	1.02 ± 0.15	20.3%	0.3 ± 0.1	0.2 ± 0.1	0.4 ± 0.2

4. Conclusion

In this study, an integrative computational and experimental approach was employed to identify natural compounds with anti-quorum sensing and anti-biofilm activity against *Klebsiella pneumoniae*. Molecular docking, pharmacophore modelling, and molecular dynamics simulations prioritised resveratrol, quercetin, and epigallocatechin gallate as potential LuxS-targeting compounds. Although quercetin and epigallocatechin gallate exhibited stronger predicted binding affinities, resveratrol demonstrated enhanced structural stability and sustained interactions with key active-site residues. This stability was reflected in experimental validation, where resveratrol showed the strongest antibacterial activity, significant inhibition of quorum sensing-associated phenotypes, and substantial reduction in biofilm formation. These findings highlight the importance of integrating binding affinity with dynamic stability and biological validation when prioritising candidate compounds. The results support the potential of resveratrol as an anti-virulence agent capable of disrupting quorum sensing and biofilm formation in multidrug-resistant pathogens.

Beyond identifying a promising lead compound, this study advances the field by demonstrating the value of combining computational prediction with experimental validation to accelerate the discovery of anti-virulence therapeutics. The integrative framework presented here provides a robust strategy for prioritizing quorum sensing inhibitors with improved translational potential. Future studies should investigate the efficacy of resveratrol in *in vivo* infection models, elucidate its molecular mechanism of LuxS inhibition, evaluate its activity in combination with conventional antibiotics and optimize its pharmacokinetic properties through structural modification or targeted delivery systems. Overall, this work underscores quorum sensing inhibition as a promising strategy for combating antimicrobial resistance and provides a foundation for the development of next-generation therapeutics against multidrug-resistant bacterial pathogens.

Declarations

Conflict of interest:

No potential conflict of interest was reported by the authors.

Author Contribution

S.K and S.A.M conceptualized and designed the study. M.J.M wrote the first draft of the paper. S.A assisted with in-vitro experiments and all authors contributed to subsequent drafts, read, and approved the final version of the manuscript.

Acknowledgement

The authors thank Professor Sandy van Vuuren from the Department of Pharmacy and Pharmacology at the University of the Witwatersrand (Wits), Johannesburg, South Africa for providing the KPn ATCC 13883 and C. violaceum strains. The authors would like to acknowledge the Centre for High Performance Computing (CHPC) server for providing supercomputing facilities based in Cape Town, South Africa to generate and analyse the in-silico data.

Data Availability

The data used/generated to support the findings of this study are available from the corresponding author on reasonable request.

References

1. Bengtsson-Palme J, Kristiansson E, Larsson DGJ (2018) Environmental factors influencing the development and spread of antibiotic resistance. FEMS Microbiol Rev 42:68–80. https://doi.org/10.1093/FEMSRE/FUX053
2. Case DA, Aktulga HM, Belfon K et al (2023) AmberTools. J Chem Inf Model 63:6183. https://doi.org/10.1021/ACS.JCIM.3C01153
3. Chen L, Wilksch JJ, Liu H et al (2020) Investigation of LuxS-mediated quorum sensing in Klebsiella pneumoniae. J Med Microbiol 69:402–413. https://doi.org/10.1099/JMM.0.001148
4. Chen TA, Chuang YT, Lin CH (2024) A Decade-Long Review of the Virulence, Resistance, and Epidemiological Risks of Klebsiella pneumoniae in ICUs. Microorganisms 2024, Vol 12, Page 2548 12:2548. https://doi.org/10.3390/MICROORGANISMS12122548
5. Deryabin D, Galadzhieva A, Kosyan D, Duskaev G (2019) Plant-Derived Inhibitors of AHL-Mediated Quorum Sensing in Bacteria: Modes of Action. Int J Mol Sci 20. https://doi.org/10.3390/IJMS20225588
6. Dixon SL, Smondyrev AM, Knoll EH et al (2006) PHASE: a new engine for pharmacophore perception, 3D QSAR model development, and 3D database screening: 1. Methodology and preliminary results. J Comput Aided Mol Des 20:647–671. https://doi.org/10.1007/S10822-006-9087-6
7. Genheden S, Ryde U (2015) The MM/PBSA and MM/GBSA methods to estimate ligand-binding affinities. Expert Opin Drug Discov 10:449–461. https://doi.org/10.1517/17460441.2015.1032936
8. Guan HH, Yoshimura M, Chuankhayan P et al (2015) Crystal structure of an antigenic outer-membrane protein from Salmonella Typhi suggests a potential antigenic loop and an efflux mechanism. Sci Rep 5:16441. https://doi.org/10.1038/SREP16441
9. Hall-Stoodley L, Costerton JW, Stoodley P (2004) Bacterial biofilms: from the natural environment to infectious diseases. Nat Rev Microbiol 2:95–108. https://doi.org/10.1038/NRMICRO821
10. Khan S, Madhi SA, Olwagen C (2024) In-silico identification of potential inhibitors against FabI protein in Klebsiella pneumoniae. J Biomol Struct Dyn 42:1506–1517. https://doi.org/10.1080/07391102.2023.2200571
11. Liang X, Chen P, Deng B et al (2022) Outcomes and Risk Factors of Bloodstream Infections Caused by Carbapenem-Resistant and Non-Carbapenem-Resistant Klebsiella pneumoniae in China. Infect Drug Resist 15:3161. https://doi.org/10.2147/IDR.S367588
12. Lipinski CA, Lombardo F, Dominy BW, Feeney PJ (2001) Experimental and computational approaches to estimate solubility and permeability in drug discovery and development settings. Adv Drug Deliv Rev 46:3–26. https://doi.org/10.1016/S0169-409X(00)00129-0
13. Maier JA, Martinez C, Kasavajhala K et al (2015) ff14SB: Improving the Accuracy of Protein Side Chain and Backbone Parameters from ff99SB. J Chem Theory Comput 11:3696–3713. https://doi.org/10.1021/ACS.JCTC.5B00255
14. Melariri H, Freercks R, van der Merwe E et al (2024) The burden of hospital-acquired infections (HAI) in sub-Saharan Africa: a systematic review and meta-analysis. EClinicalMedicine 71:102571. https://doi.org/10.1016/J.ECLINM.2024.102571
15. Murray CJ, Ikuta KS, Sharara F et al (2022) Global burden of bacterial antimicrobial resistance in 2019: a systematic analysis. Lancet 399:629–655. https://doi.org/10.1016/S0140-6736(21)02724-0
16. Olwagen CP, Izu A, Khan S et al (2025) Genomic relatedness of colonizing and invasive disease Klebsiella pneumoniae isolates in South African infants. Sci Rep 2025 15(1):8043. https://doi.org/10.1038/s41598-025-92517-4
17. Roe DR, Cheatham TE (2013) PTRAJ and CPPTRAJ: Software for Processing and Analysis of Molecular Dynamics Trajectory Data. J Chem Theory Comput 9:3084–3095. https://doi.org/10.1021/CT400341P

18. Roy V, Adams BL, Bentley WE (2011) Developing next generation antimicrobials by intercepting AI-2 mediated quorum sensing. Enzyme Microb Technol 49:113–123. https://doi.org/10.1016/j.enzmictec.2011.06.001
19. Rutherford ST, Bassler BL (2012) Bacterial Quorum Sensing: Its Role in Virulence and Possibilities for Its Control. Cold Spring Harb Perspect Med 2:a012427. https://doi.org/10.1101/CSHPERSPECT.A012427
20. Salsbury FR (2010) Molecular dynamics simulations of protein dynamics and their relevance to drug discovery. Curr Opin Pharmacol 10:738–744. https://doi.org/10.1016/J.COPH.2010.09.016
21. Schauder S, Shokat K, Surette MG, Bassler BL (2001) The LuxS family of bacterial autoinducers: biosynthesis of a novel quorum-sensing signal molecule. Mol Microbiol 41:463–476. https://doi.org/10.1046/J.1365-2958.2001.02532.X
22. Shelley JC, Cholleti A, Frye LL et al (2007) Epik: a software program for pK(a) prediction and protonation state generation for drug-like molecules. J Comput Aided Mol Des 21:681–691. https://doi.org/10.1007/S10822-007-9133-Z
23. Thakur V, Chalana A, Gupta A et al (2025) Dual-species biofilm of MDR Acinetobacter baumannii and Klebsiella pneumoniae are susceptible to colistin-rifamycin combination therapy. J Appl Microbiol 136. https://doi.org/10.1093/JAMBIO/LXAF171
24. World Health Organization (2024) WHO Bacterial Priority Pathogens List, 2024- Bacterial pathogens of public health importance to guide research, development and strategies to prevent and control antimicrobial resistance. World Health Organ 1–72

Figures

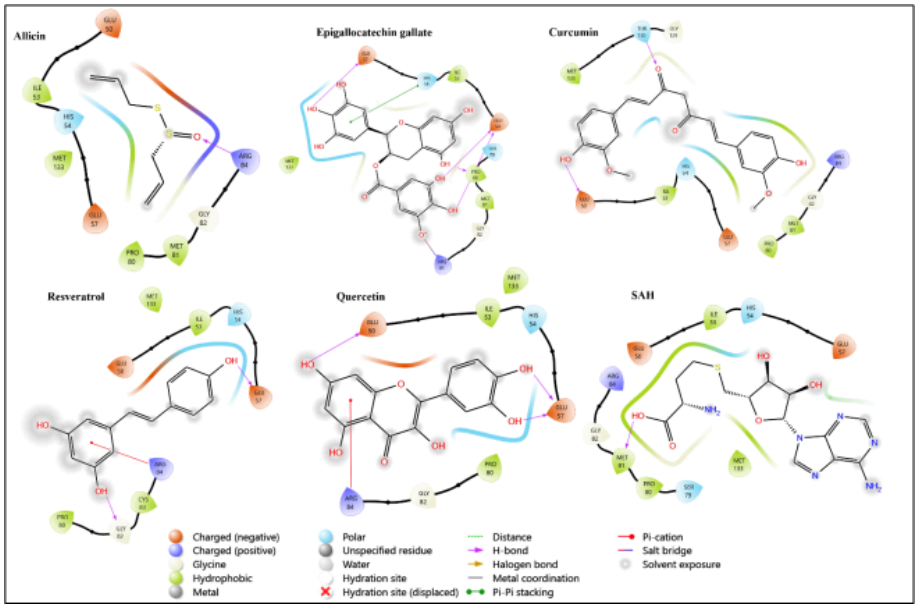


Figure 1

2D interaction profiles of selected natural compounds within the LuxS active site.

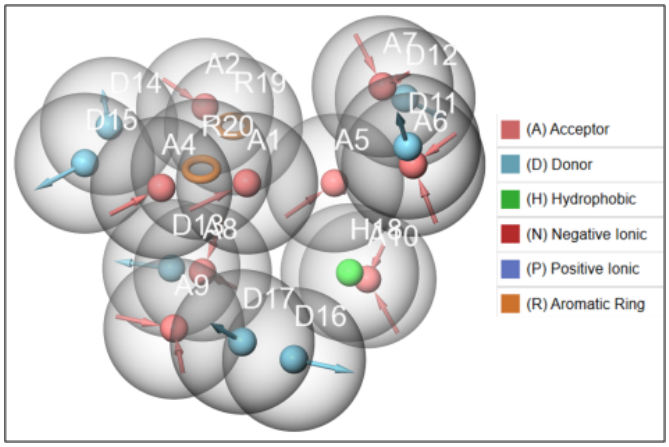


Figure 2

Structure-based e-pharmacophore model of the LuxS active site derived from the bound conformation of SAH. The 3D pharmacophore illustrates key interaction features, including hydrogen bond acceptors (red arrows), hydrogen bond donors (blue arrows), and aromatic ring interactions (orange spheres), with the ligand structure embedded within defined excluded volumes (grey spheres) representing steric constraints.

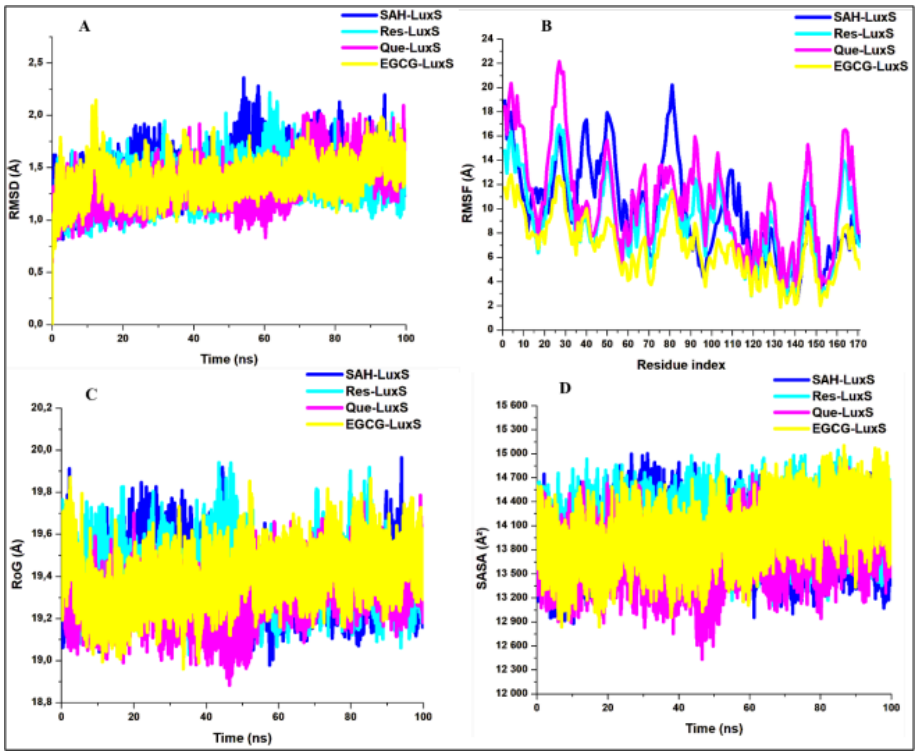


Figure 3

Structural dynamics of LuxS protein in complex with studied inhibitors and control inhibitors. **A:** RMSD in Å calculated for Carbon backbone atoms in LuxS protein in complex with S-adenosylhomocysteine (SAH), Resveratrol (Res), Quercetin (Que) and Epigallocatechin gallate (EGCG); **B:** RMSF values in Å calculated for LuxS protein in complex with S-adenosylhomocysteine (SAH), Resveratrol (Res), Quercetin (Que) and Epigallocatechin gallate (EGCG); **C:** Rg values in Å calculated for LuxS protein in complex with S-adenosylhomocysteine (SAH), Resveratrol (Res), Quercetin (Que) and Epigallocatechin gallate (EGCG); **D:** SASA values in Å2 calculated for LuxS protein in complex with S-adenosylhomocysteine (SAH), Resveratrol (Res), Quercetin (Que) and Epigallocatechin gallate (EGCG) after 100 ns of MD simulations.

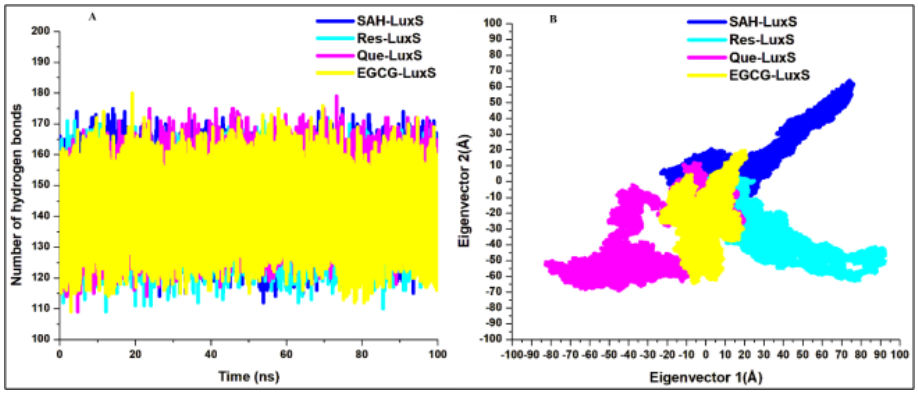


Figure 4

A: 2-dimensional representation of intra-molecular hydrogen bond formation for LuxS protein in complex with S-adenosylhomocysteine (SAH), Resveratrol (Res), Quercetin (Que) and Epigallocatechin gallate (EGCG) calculated after 100 ns of MD simulations. **4B** PCA plot constructed by eigenvector 1 vs eigenvector 2 for for LuxS protein in complex with S-adenosylhomocysteine (SAH), Resveratrol (Res), Quercetin (Que) and Epigallocatechin gallate (EGCG) showing the positive and negative residual movements over 100 ns MD trajectories.

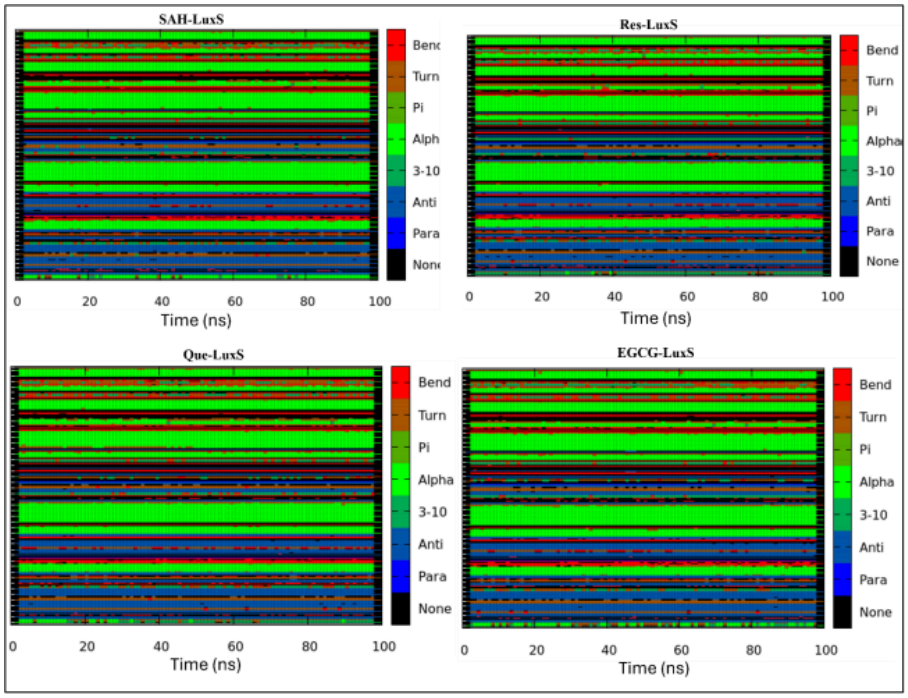


Figure 5

Secondary structure analysis of LuxS protein in complex with the studied inhibitors and the control inhibitor calculated after 100 ns of MD trajectories.

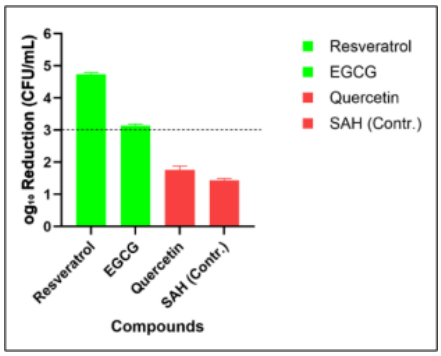


Figure 6

Effect of selected compounds on bacterial viability against KPn ATCC 13883: Bar chart showing $\log_{10}$ reduction in viable CFU/mL at the Minimum Inhibitory Concentration (MIC). Compounds achieving ≥3 $\log_{10}$ reduction (green bars) are classified as bactericidal, while those with <3 $\log_{10}$ reduction (red bars) are classified as bacteriostatic. The horizontal dashed line marks the bactericidal threshold (3 $\log_{10}$ reduction). Resveratrol and EGCG demonstrated bactericidal activity, while quercetin and SAH were bacteriostatic. Error bars represent SD (n=3).

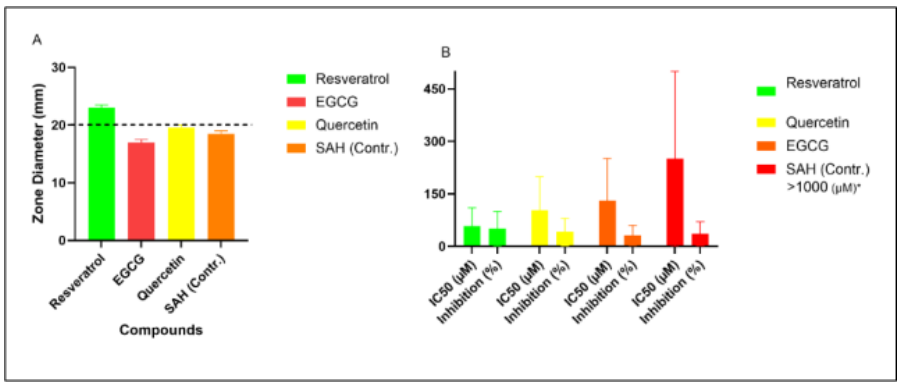


Figure 7

Qualitative and Quantitative Anti-QS Activity Against C. violaceum. (A) Zones of violacein inhibition produced by natural compounds at MIC concentrations in the well diffusion assay. The dashed line at 20 mm indicates the threshold for Susceptible (S) classification (>20 mm = S; 15–19 mm = I; <14 mm = R). Resveratrol (23.0 mm) was the only compound classified as Susceptible. (B) Correlation between IC_{50} values (µg/mL) and percent inhibition at MIC for each compound. Lower IC_{50} values indicate higher potency, with resveratrol showing the lowest IC_{50} (110 µM) and highest percent inhibition (99.8%). Data represent mean ± SD (n=3).

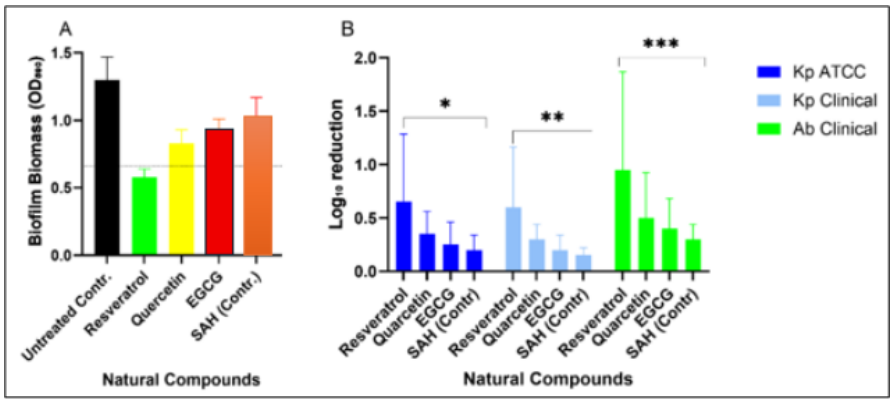


Figure 8

Effect of Natural Compounds on Dual-Species Biofilm Formation by KPn and Aba. (A) Biofilm biomass (OD_{590}) after treatment with natural compounds at ½ MIC. Resveratrol showed the highest inhibition (54.7%, green bar), followed, quercetin (35.2%), EGCG (29.7%), and SAH (20.3%). The horizontal dashed line indicates the 50% inhibition threshold for MBIC definition. (B) Log_{10} reduction in viable counts of each species recovered on selective media. Aba (green bars) showed greater susceptibility to all compounds compared to KPn ATCC 13883 (blue bars) and clinical isolate (light blue bars). Data represent mean ± SD (n = 3). *p < 0.05, **p < 0.01, ***p < 0.001 compared to untreated control (one-way ANOVA with Dunnett's post-hoc test).

Supplementary Files

This is a list of supplementary files associated with this preprint. Click to download.

- floatimage1.png